

## State-selective charge exchange in collisions of multiply charged ions with H<sub>2</sub>

N. D. Cariato<sup>✉\*</sup> and S. Otranto<sup>✉†</sup>

*Instituto de Física del Sur (IFISUR), Departamento de Física, Universidad Nacional del Sur (UNS),  
CONICET, Av. L. N. Alem 1253, B8000CPB-Bahía Blanca, Argentina*

 (Received 29 May 2024; revised 6 August 2024; accepted 26 August 2024; published 9 September 2024)

In this work, an improved classical trajectory Monte Carlo method is introduced to describe collisions of multiply charged ions with H<sub>2</sub> molecules by merging two hydrogenic three-body models, conceived to improve the H(1s) electronic radial distribution, into the five-body treatment of Wood and Olson. Present results are contrasted against recently reported laboratory data and the multichannel Landau-Zener method for Ne<sup>9+</sup> and O<sup>6+</sup> projectiles at intermediate to low impact energies. A reasonable agreement with the data is obtained at the *n*-state selective level when considering a hydrogenic model that relies on an expansion over different nuclear charges. Complementary results for He<sup>2+</sup> and Fe<sup>26+</sup> projectiles suggest that discrepancies among these models accentuate as the projectile charge is increased and the collision energy is lowered, and highlight the need for further joint experimental and theoretical studies.

DOI: [10.1103/PhysRevA.110.032805](https://doi.org/10.1103/PhysRevA.110.032805)

### I. INTRODUCTION

In the past few decades, charge exchange processes have been shown to play a significant role in astrophysical environments. This process has been found to be at a great extent responsible for the emission lines that originate in the electronic cascade that follows the interaction of charged ions with comets, planetary atmospheres, the heliosphere, astrospheres of stars, supernova remnants, and highly ionized regions of the interstellar medium [1–9].

Among the relevant gaseous targets, H<sub>2</sub> is the most abundant molecule in the universe and controls much of the chemistry in the interstellar medium [10]. During the last decades, charge exchange processes in collisions of ions with H<sub>2</sub> have been experimentally studied over a wide impact energy range [11–37]. Laboratory data focused on the determination of single and double charge exchange total cross sections, *n*-resolved state-selective charge exchange, and the emission lines resulting from the cascading process. To benchmark these studies, a diverse set of theoretical models have been implemented. Among them, we can cite diverse three-body and five-body versions of the classical-trajectory Monte Carlo (CTMC) method [38–41], the Bohr-Lindhard model [42], the model potential method [43], the linear combinations of molecular orbitals (LCMO) method [44], the atomic-orbital close-coupling (AOCC) method [45,46], the semiclassical molecular-orbital close-coupling (MOCC) method [47], the two-active-electron three-center semiclassical asymptotic-state close-coupling (SCASCC) method [48], the single-particle time-dependent Schrödinger equation (TDSE) [49], and the multichannel Landau-Zener (MCLZ) method [50,51].

The CTMC method has been routinely used to describe ion-atom and ion-molecule collisions during the past four decades. In contrast to numerically intensive quantum mechanical methods, this method does not rely on extensive basis sets to deal with highly charged projectiles and provides electron capture cross sections for high-lying *n* values. For hydrogen atoms in the ground state, its success has been partially attributed to the fact that in the microcanonical description the classical and quantum mechanical momentum distributions for the target electron are identical. The first molecular multicenter CTMC model for H<sub>2</sub> was proposed by Meng *et al.* in 1989 [39]. In their work, a two-electron distribution was constructed in terms of two microcanonical distributions, one for each electron. A decade later, Wood and Olson introduced a five-body model to study double ionization of H<sub>2</sub> by 3.6 MeV/u Se<sup>28+</sup> and 1 GeV/u U<sup>92+</sup> [41]. In this case, the H<sub>2</sub> molecule was initialized in terms of two independent hydrogen atoms united by means of a Morse potential. As one of the electrons was removed from the target (i.e., acquired a positive energy with respect to its parent nucleus), the interactions among all particles were turned on by means of a switching function. This model has also been used by our group to describe single electron capture in He<sup>+</sup> collisions at intermediate to low impact energies [31]. In this case, very good agreement was found with the *n*-state selective capture cross sections measured by the reaction microscope setup at the Bariloche Laboratory in Argentina.

In this work, we introduce a five-body CTMC method for H<sub>2</sub>, which provides an improved representation of the target system compared to the microcanonical ensemble used by Wood and Olson. Two hydrogenic distributions, conceived to provide a more accurate representation of the radial distribution for H(1s) are implemented and extend the electronic distribution of H<sub>2</sub> to larger distances. In Sec. II we describe the theoretical method and its implementation. In Sec. III A, results for state-selective charge exchange are shown and

\*Contact author: [nelson.cariato@uns.edu.ar](mailto:nelson.cariato@uns.edu.ar)

†Contact author: [sotranto@uns.edu.ar](mailto:sotranto@uns.edu.ar)

contrasted with other five-body CTMC models as well as to recently reported experimental data for  $\text{Ne}^{9+}$  and  $\text{O}^{6+}$  projectiles. We widen the scope of our study by analyzing the one-electron capture total and  $np$ -state selective cross sections predicted by these models for  $\text{He}^{2+}$  projectiles at impact energies in the range 7–200 keV/u and the  $n$ -state selective cross sections for  $\text{Fe}^{26+}$  projectiles at a typical solar wind energy. Finally, in Sec. IV, conclusions and outlook are drawn.

## II. THEORETICAL METHODS

In what follows we describe the five-body CTMC models employed in this work to describe collisions between charged ions and  $\text{H}_2$  molecules. In all cases, the initial state of the  $\text{H}_2$  molecule is initially described by two independent hydrogen atoms held together by a Morse potential with the experimental vibrational ground-state energy [31,41]. Each electron is bound to only one nucleus. The electron-electron interaction, as well as the interaction of each electron with the other nucleus is not taken into account in the initial stage of the collision.

*5CTMC (Wood and Olson model).* In the original version of the five-body CTMC, each electron is initialized bound to its parent nucleus with positions and momenta obtained from microcanonical distributions. In this description, the electron momentum distribution for each hydrogen atom is found in perfect agreement with its quantum mechanical counterpart as already stated. However, the exponential decreasing behavior expected at large distances is not reproduced due to the existence of a classical return point. As a result, the electronic density of the  $\text{H}_2$  molecule exhibits a sharp cutoff in its spatial extension.

*E-CTMC method.* Improved descriptions of the CTMC method were designed for  $\text{H}(1s)$  in order to predict an electronic radial distribution in concordance with the quantum mechanical counterpart. Eichenaur *et al.* used the Wigner function for the initial distribution of the coordinates and momenta of the electron instead of the microcanonical phase space distribution [52]. Simultaneously, Hardie and Olson fitted the quantum mechanical radial distribution by means of a linear combination of microcanonical distributions corresponding to different ionization potentials  $E_i$  [53]. The microcanonical radial distributions are obtained by integrating the microcanonical phase space distribution  $f(\mathbf{r}, \mathbf{k}) = \mathcal{N} \delta(E_i - k^2/2\mu - Z/r)$  over the momentum coordinates and the electron angular coordinates, giving:

$$\rho(r, E_i) = \frac{16E_i^3 r^2}{\pi Z^3} \sqrt{\frac{Z}{E_i r} - 1}. \quad (1)$$

Here,  $\mathcal{N}$  is a normalization constant,  $Z$  is the nuclear charge,  $\mathbf{r}$  and  $\mathbf{k}$  are the electron's position and momentum with respect to the nucleus, respectively, and  $\mu$  is the relative mass of the electron-nucleus system. Soon after, Cohen proposed a new classical phase-space distribution, which also considered an energy distribution for the bound electron obtaining a radial distribution coincident with the quantum mechanical description while still providing a good approximation to the momentum distribution [54]. We hereafter refer to these models as E-CTMC models, noting that according to

TABLE I. Weight factors ( $\alpha_i$ ) for the  $1s$  orbitals on each nucleus of H.

$Z_i$	$\alpha_i$
0.500	0.07240
0.625	0.07658
0.750	0.09665
0.875	0.09230
1.000	0.16204
1.250	0.17971
1.500	0.13019
1.750	0.08071
2.000	0.06475
2.500	0.04493

extensive use and evaluation for more than four decades, they lead in principle to very similar results [54–56].

In this work we use the methodology introduced by Cohen [54]. Differences with the 5CTMC method amount to the initialization of each electron in its parent nucleus. The implemented procedure extends the electronic density in the  $\text{H}_2$  molecule to larger distances compared to the microcanonical prescription.

*Z-CTMC method.* An alternative model termed Z-CTMC was introduced by our group a decade ago with the aim of improving the radial distribution when considering processes such as charge exchange, which are particularly sensitive to the ionization potential of the target. In this model, the radial distribution for  $\text{H}(1s)$  was fitted by means of a linear combination of microcanonical distributions by using the nuclear charge as the expansion parameter, instead of the ionization potential [56,57]:

$$\rho(r, Z_i) = \frac{16E_0^3 r^2}{\pi Z_i^3} \sqrt{\frac{Z_i}{E_0 r} - 1}, \quad (2)$$

$E_0$  being the ionization potential of the hydrogen ground state. Overall, and compared to the E-CTMC predictions, the Z-CTMC method led  $\text{H}(1s)$  to closer agreement to the AOCC results of Igenbergs *et al.* [58,59].

In order to extend the Z-CTMC method for the  $\text{H}_2$  molecule in its ground state, we keep the ionization potential as a fixed parameter and we approximate the quantum mechanical radial distribution for each hydrogen atom conforming the molecule as a linear combination of  $N$  classical microcanonical radial distributions  $\rho(r, Z_i)$ :

$$\rho(r) = \sum_{i=1}^N \alpha_i \rho(r, Z_i). \quad (3)$$

Here,  $\alpha_i$  are the weight factors for the different distributions associated with the different  $Z_i$  values considered. Explicit values are provided in Table I.

Since we have a sum of  $N = 10$  classical radial distributions for each hydrogen atom, the molecular structure is recovered by considering the 100 resulting combination terms that, due to symmetry, can be reduced to 55 in order to reduce the computational cost. In Fig. 1 we show in logarithmic scale the electron density ( $P$ ) obtained in the molecular plane

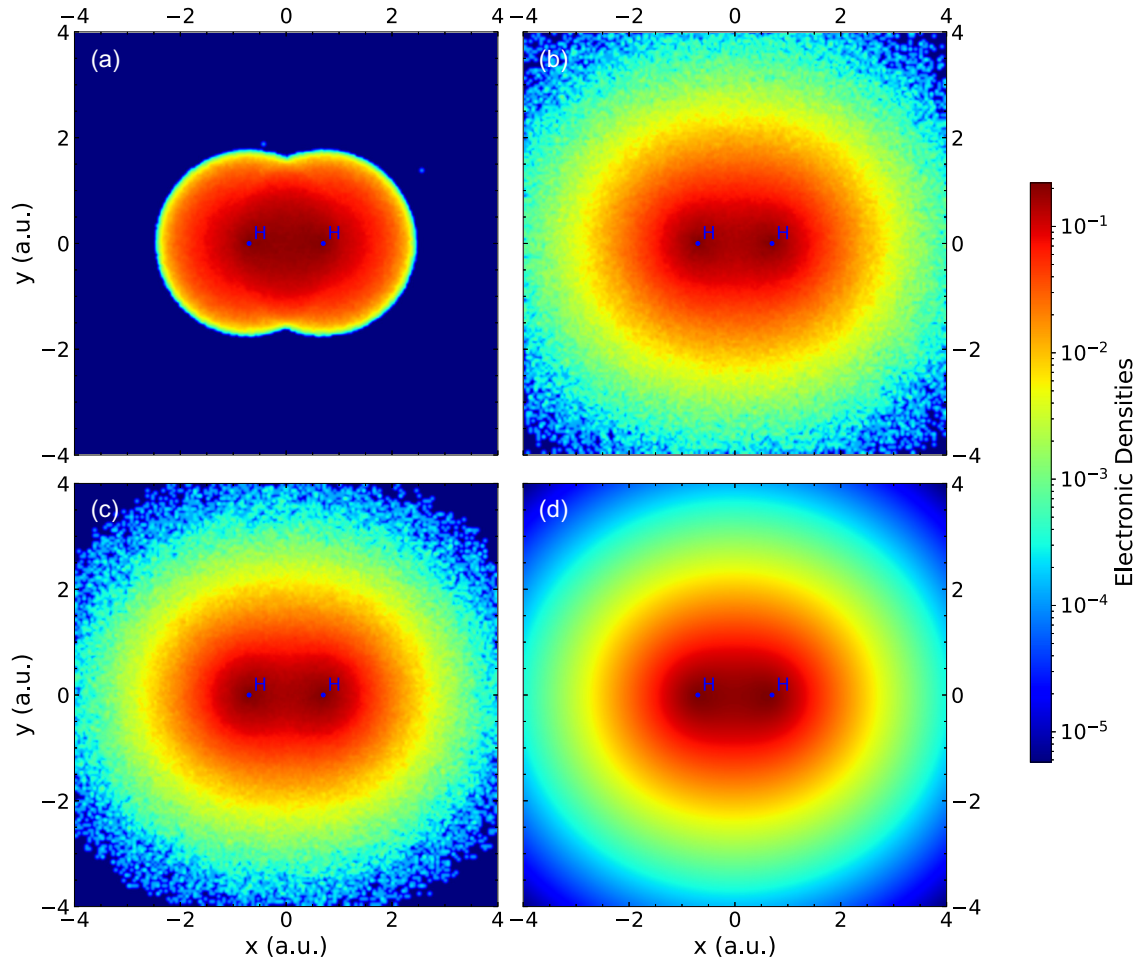


FIG. 1. Logarithmic electronic densities in the  $xy$  molecular plane for  $H_2$ . (a) Microcanonical 5CTMC method, (b) E-CTMC method, (c) present Z-CTMC method, and (d) quantum mechanical description [60].

defined by the molecular axis ( $x$ ) and one of the perpendicular directions ( $y$ ). The statistical description obtained with 5CTMC, E-CTMC, and Z-CTMC are compared to the quantum mechanical description obtained from a molecular orbital wave function [60]:

$$P(x, y) = \int d\mathbf{r}_2 dz |\Psi(\mathbf{r}, \mathbf{r}_2)|^2, \quad (4)$$

where  $\mathbf{r} = (x, y, z)$  and  $\mathbf{r}_2 = (x_2, y_2, z_2)$ . For the classical trajectory models, the electron density is obtained by turning off the projectile and taking a picture of the evolving trajectories at any given time. The  $(x, y)$  ordinate pairs corresponding to each electron are registered and binned over the spatial grid. The distribution is normalized by requiring that

$$\int dx dy P(x, y) = 1. \quad (5)$$

The hydrogenic models, E-CTMC and Z-CTMC, provide an improved description with respect to the microcanonical model, exhibiting a more spatially extended electronic density.

At the beginning of the simulation the center of mass of the target is considered to be frozen and is located at the origin of the coordinate system. Hamilton's equations are written in terms of Cartesian coordinates and are numerically solved

by means of a fourth-order Runge-Kutta-Hill method with adaptive step size. For our present purposes, we consider a nonoriented molecule. Hence, the positions and momenta of the electrons and the nuclei are randomly rotated by means of Euler angles. As the collision process proceeds, the energy of each electron with respect to its parent nucleus is checked in every time step. Whenever an electron reaches the continuum, the electron-electron and the electron-other nucleus interactions are turned on smoothly in the Hamiltonian by means of the switching function  $f(t) = 1 - e^{-\tau(t-t_0)}$ . Here,  $\tau$  is the time constant and  $t_0$  is the instant of electron removal. The value of  $\tau$  has been evaluated over the range (0.1,100) without obtaining significant changes in the electron capture cross sections reported in this work. Therefore, it has been arbitrarily set to  $\tau = 0.1$  a.u.

The simulation is stopped once the projectile recedes from the reaction region and the collisional process can be considered as finished. The evaluation of the relative energy of the electrons with respect to the nuclei allows characterizing the nature of the collisional event and determining whether an electron has been excited, ionized, or captured. For the latter, a classical number  $n_c$  is obtained from the binding energy  $E_p$  of the electron relative to the projectile by

$$E_p = -Z_p^2/(2n_c^2), \quad (6)$$

where  $Z_p$  is the charge of the projectile core as long as bare projectiles are considered. These classical  $n_c$  values are then related to the specific quantum level  $n$  according to the relationship derived by Becker and MacKellar [61],

$$[n(n-1)(n-1/2)]^{1/3} \leq n_c < [n(n+1)(n+1/2)]^{1/3}. \quad (7)$$

From the normalized classical angular momentum  $l_c = (n/n_c)(\mathbf{r} \times \mathbf{k})$ , where  $\mathbf{r}$  and  $\mathbf{k}$  are the captured electron position and momentum, respectively, relative to the projectile, we relate  $l_c$  to the orbital quantum number  $l$  of the final state by  $l \leq l_c \leq l+1$ .

For dressed projectiles we have used the central potential model developed by Green *et al.* [62] from Hartree-Fock calculations and, later on, generalized by Garvey *et al.* [63] to describe the interaction of the projectile with the other particles. To calculate the  $n$ -state selective capture cross sections, we have used the model developed by Schultz *et al.* [64] and that we successfully implemented in our previous work on  $\text{He}^+ + \text{H}_2$  [31].

The  $(n, l)$  state-selective capture cross section for the 5CTMC and E-CTMC methods is defined as:

$$\sigma^{\text{cap}} = \frac{N(n, l)}{N_{\text{tot}}} \pi b_{\text{max}}^2, \quad (8)$$

where  $N(n, l)$  is the number of events associated with the process of capture to the  $(n, l)$  state,  $N_{\text{tot}}$  is the total number of trajectories integrated, and  $b_{\text{max}}$  is the impact-parameter value beyond which the probability to collect events is negligibly small.

For the Z-CTMC model, the capture cross sections must consider the contribution of all linear combinations, and are therefore defined by

$$\sigma^{\text{cap}} = \sum_i \sum_j \alpha_i \alpha_j \sigma_{ij}^{\text{cap}}, \quad (9)$$

where  $\sigma_{ij}^{\text{cap}}$  are the set of cross sections for a given combination of the expansion terms corresponding to nuclear charges  $Z_i$  and  $Z_j$ . In other words,  $\sigma_{ij}^{\text{cap}}$  is the electron capture cross section corresponding to the simulation in which one of the electrons is initialized with the microcanonical distribution  $f(\mathbf{r}_1, \mathbf{k}_1) = \mathcal{N} \delta(E_0 - k_1^2/2\mu - Z_i/r_1)$  to its parent nucleus, while the other electron, bound to the other nucleus, is initialized by means of the microcanonical distribution  $f(\mathbf{r}_2, \mathbf{k}_2) = \mathcal{N} \delta(E_0 - k_2^2/2\mu - Z_j/r_2)$ , respectively. It is worth noting that an identical expression is obtained for the E-CTMC in the Hardie and Olson's version, since it considers an expansion of microcanonical distributions corresponding to different ionization potentials (IP) [53].

Whenever a double electron capture event is detected during the simulation, the electron-electron interaction is suddenly turned off to avoid the classical autoionization of the ion. As a result, this double capture event is characterized by an electron in the  $(n_1, l_1)$  state and the other in the  $(n_2, l_2)$  state. While these events naturally lead for highly charged ions to either autoionization or double radiative decay, these subsequent processes are not inherently included in the classical treatment and a subsequent Auger decay scheme needs to be implemented. The Auger decay scheme used in this work is based on that developed by Ali *et al.* [65] for collisions involving argon ions with argon atoms and that we adapted

in previous work for electron capture processes involving highly charged ions and CO, Ne, Ar, and Kr targets [66,67]. This strategy successfully reproduced the line emission cross sections obtained at NIST following  $\text{Ne}^{10+}$ ,  $\text{Ar}^{18+}$ , and  $\text{Kr}^{36+}$  collisions on Ar at 4 keV/u [68], those obtained at the Berlin-EBIT for  $\text{Ar}^{18+}$  collisions on Ar at collision energies of 18 eV/u and 218 eV/u [69], and those obtained by Trassinelli *et al.* for  $\text{Ar}^{17+}$  collisions on Ar at 7 keV/u [70]. For  $\text{H}_2$  target, this scheme can be summarized as follows:

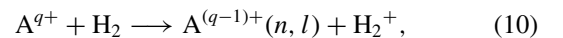
(1) Events corresponding to an asymmetric doubly excited state ( $|n_2 - n_1| \geq 2$ ), are characterized as double radiative decay and lead to true double capture (DEC).

(2) For nearly symmetric excited states ( $|n_2 - n_1| < 2$ ), an Auger process takes place. We characterize this process as autoionizing double capture (A2C). The decaying electron falls to a well-established  $n$  level according to the energy equation while the other is assumed to proceed to the nearest continuum limit with unit probability. The electronic angular momentum of the decaying electron is determined throughout the Auger process by requiring the preservation of its respective orbital eccentricity, which in practical terms implies that the initial  $(n_i, l_i)$  and final  $(n_f, l_f)$  states of the decaying electron satisfy  $l_f = l_i(n_f/n_i)$  [67].

### III. RESULTS AND DISCUSSION

#### A. State-selective electron capture in $\text{O}^{6+}$ and $\text{Ne}^{9+}$ collisions on $\text{H}_2$

First, we benchmark the present method by analyzing  $n$ -resolved state-selective nondissociative single electron capture ( $\text{SEC}_{nd}$ ) processes for  $\text{Ne}^{9+}$  and  $\text{O}^{6+}$  projectiles for which recent COLTRIMS experimental data from the Lanzhou group are available [36,37]. Since these  $\text{SEC}_{nd}$  were obtained from the coincidence detection of the residual molecular  $\text{H}_2^+$  ion and the projectile, autoionizing events originated in double capture processes, which ultimately lead to a change of the projectile charge state by one unit are not included in the data. Therefore, in our simulations we have only considered those events that comply with the reaction:



where A is the projectile element and  $q$  its charge state.

In Fig. 2, we display the obtained  $\text{SEC}_{nd}$   $n$ -state cross sections in  $\text{Ne}^{9+}$  collisions on  $\text{H}_2$  as a function of the binding energy difference  $Q = \epsilon_i - \epsilon_f$  of the active electron before and after collision, spanning the impact energy range 2.25–24.75 keV/u. In this expression,  $\epsilon_i$  and  $\epsilon_f$  are the binding energies of the active electron, in the initially ground-state target and finally excited projectile ion, respectively. Theoretically, each capture  $n$  state is associated with its corresponding  $Q$  value through an average procedure over the eigenvalues  $E_{n,l}$  that were calculated by numerically solving the one-electron Hamiltonian corresponding to a Garvey potential for the  $\text{Ne}^{9+}$  ion. The reported experimental spectra, given in arbitrary counts, was extracted from the paper and renormalized using the reported relative cross section (Table 2 in Ref. [36]) for the  $n = 5$  level. A background subtraction procedure was implemented at this point. The theoretical relative and

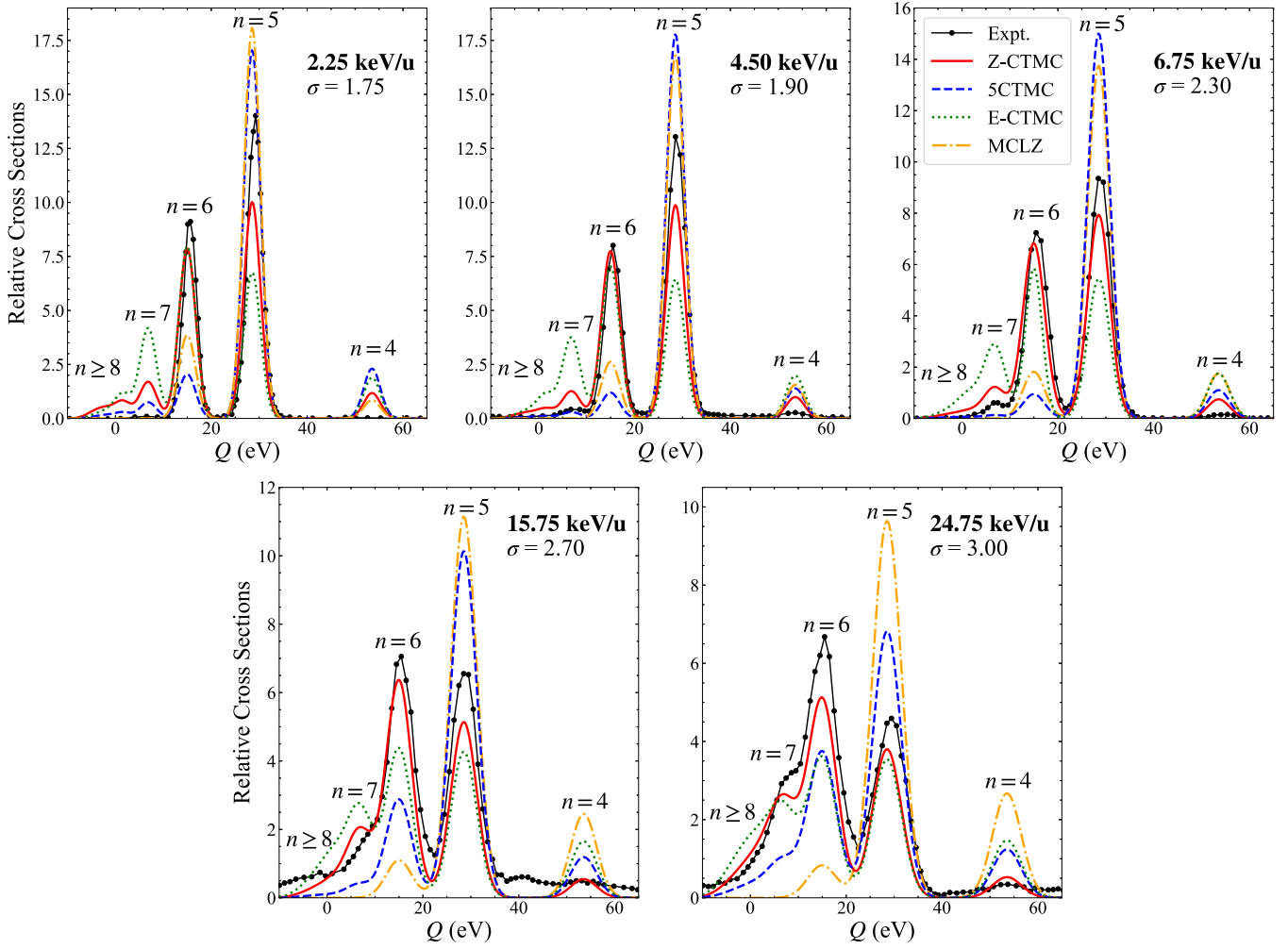


FIG. 2. Nondissociative single electron capture  $Q$  spectra for  $\text{Ne}^{9+}$  collisions on  $\text{H}_2$ . The theoretical predictions of the Z-CTMC model are contrasted to those provided by the E-CTMC and 5CTMC methods. The MCLZ results and the experimental data are those reported in Ref. [36].

absolute  $n$ -state selective  $\text{SEC}_{nd}$  cross sections are shown in Tables II and III, respectively.

Theoretical results from the present 5CTMC, Z-CTMC and the E-CTMC methods, are compared to the experimental relative  $\text{SEC}_{nd}$  cross sections and the MCLZ calculations reported in Ref. [36]. To mimic the experimental resolution, theoretical cross sections have been convoluted by means of Gaussian functions. The Gaussian width value  $\sigma$  is indicated in each case and was chosen in order to provide the best visual fit to the width of the experimental  $n = 5$  peak.

A quick survey of the experimental trends clearly shows a distribution maximizing at  $n = 5$  closely followed by  $n = 6$  at impact energies lower than 6.75 keV/u while  $n = 6$  is dominant at 15.75 keV/u and 24.75 keV/u. Electron capture to  $n \geq 7$  is negligible at 2.25 keV/u but gains relevance with increasing impact energy. Very minor traces of electron capture to  $n = 4$  can be also seen at 4.5 keV/u and 6.75 keV/u. Instrumental resolution seems to play a role for the 15.75 keV/u and 24.75 keV/u cases, turning difficult any specific assessment on the population of this level.

Regarding the theoretical predictions, we observe that the MCLZ distribution reported by Xu *et al.* maximizes at  $n = 5$

in the whole energy range explored. The agreement with the data worsens as the impact energy increases, with clear dominance of the low  $n$  values in clear discrepancy with the experimental trends. No population of  $n \geq 7$  levels is predicted at the impact energy range explored. On the other hand, the 5CTMC model tends to overestimate the experimental electron capture to  $n = 5$  while it underestimates the experimental data, the dominance of electron capture to  $n = 5$  extends over the whole impact energy range explored.

For the E-CTMC model, we observe that the maximum of the distribution is shifted to  $n = 6$  at all impact energies, although its population difference with electron capture to  $n = 5$  decreases with increasing energy. Overall, the  $n$  distribution looks much wider than that experimentally reported. This could obey to the fact that the most populated projectile  $n$  level in charge-exchange processes is roughly given by the  $\sqrt{13.6/\text{IP}} q^{3/4}$  scaling law (where  $q$  is the projectile charge and IP is the ionization potential expressed in eV) [71]. A methodology based on a set of microcanonical distributions involving different IP values is expected to lead to a wider overall  $n$  distribution, depending on the relative weight of the

TABLE II. Comparison of measured and calculated relative cross sections of the  $n$ -resolved state-selective  $\text{SEC}_{nd}$  process in  $\text{Ne}^{9+}$  collisions with  $\text{H}_2$ .

Energy (keV/u)	$n$	$\sigma_{\text{Expt.}}^{\text{rel}}(\%)$	$\sigma_{\text{Z-CTMC}}^{\text{rel}}(\%)$	$\sigma_{\text{5CTMC}}^{\text{rel}}(\%)$	$\sigma_{\text{E-CTMC}}^{\text{rel}}(\%)$	$\sigma_{\text{MCLZ}}^{\text{rel}}(\%)$
2.25	3		0.06	0.07	0.44	
	4		5.16	10.11	8.29	3.72
	5	61.29(0.90)	43.97	74.79	29.64	79.34
	6	37.78(0.75)	34.51	9.00	34.93	16.93
	7	0.94(0.29)	7.43	3.28	18.31	$5.86^{-4}$
	$\geq 8$		8.87	2.75	8.39	
4.50	3		0.03	0.04	0.57	
	4	1.19(0.84)	4.72	6.63	9.44	7.41
	5	62.36(0.79)	47.06	84.70	30.64	80.04
	6	34.25(0.83)	36.95	5.69	33.55	12.52
	7	2.21(0.95)	5.98	1.41	17.80	$4.30^{-4}$
	$\geq 8$		5.26	1.53	8.00	
6.75	3		0.02	0.01	0.65	
	4	1.72(0.31)	4.30	6.36	10.11	10.15
	5	53.63(0.53)	45.77	86.52	31.39	79.28
	6	40.97(0.51)	39.39	5.46	33.69	10.48
	7	3.68(0.31)	6.92	0.74	16.35	$3.58^{-4}$
	$\geq 8$		3.60	0.91	8.11	
15.75	3		0.03	0.03	0.80	
	4	1.90(0.81)	3.70	8.05	11.19	16.60
	5	44.56(1.10)	34.79	68.59	28.91	75.42
	6	44.73(1.13)	43.00	19.48	29.51	7.41
	7	8.81(0.87)	13.12	2.69	17.34	$2.50^{-4}$
	$\geq 8$		5.36	1.16	12.25	
24.75	3		0.05	0.09	0.98	
	4	2.47(0.72)	3.98	9.32	11.07	20.09
	5	34.70(0.96)	28.59	51.30	26.66	72.51
	6	43.84(1.02)	38.12	28.09	26.82	6.25
	7	18.99(0.81)	17.76	6.90	16.18	$2.10^{-4}$
	$\geq 8$		11.50	4.30	18.29	

terms involving IP values lower than that considered physically correct.

Now moving to the Z-CTMC model, the  $n$  distribution maximizes at  $n = 5$  followed closely by  $n = 6$  at the three lower impact energies considered. In concordance with the experimental trends the dominance reverses at the two higher energies considered. A minor fraction of  $\text{SEC}_{nd}$  is predicted to populate  $n = 4$ , a behavior also predicted by the other theoretical models. All the classical trajectory methods hereby analyzed predict, at a different extent, the population of  $n$  levels beyond  $n = 7$ .

Similarly, Fig. 3 shows the relative  $n$ -state selective cross sections as a function of  $Q$  for  $\text{O}^{6+}$  collisions on  $\text{H}_2$  spanning the impact energy range 19.5–100 keV/u. In this case, the different theoretical methodologies are compared to the recent measurements reported by Cao *et al.* [37]. The experimental data were normalized in the same way as was done with  $\text{Ne}^{9+}$ , with the exception that here the peak at  $n = 3$  was used to normalize the extracted spectra, due to its isolation from other structures. The theoretical relative and absolute  $n$ -state selective  $\text{SEC}_{nd}$  cross sections are shown in Tables IV and V, respectively.

At the lowest energy considered, the experimental spectra exhibit a maximum at  $n = 4$  followed in intensity by

$n = 5$  at the lowest impact energy explored. Minor structures are visible for  $n \geq 6$  and  $n = 3$ . As the impact energy increases, the dominance of the  $n = 4$  structure attenuates and the relative population of states corresponding to  $n \geq 6$  gains relevance becoming the dominant structure already at 75 keV/u.

Regarding the theoretical descriptions, at the lowest impact energy the 5CTMC method leads to good agreement with the data at the maximum capture peak  $n = 4$ . However, it clearly underestimates the  $n = 5$  and  $n \geq 6$  structures while at the same time it overestimates the  $n = 3$  population. As the impact energy increases, this method predicts the maximum of the distribution at  $n = 4$  but the dominance over the other  $n$  values is reduced. The E-CTMC, on the other hand, is in good agreement with measurements at  $n = 3$  in the range 19.5–75 keV/u, but the description of the experimental spectra is acceptable only at impact energies greater than 75 keV/u. At lower impact energies, the distribution exhibits a more pronounced population of large  $n$  values and, overall, a wider spectra. The Z-CTMC method is the one that provides the closest agreement with the measurements when analyzing the whole energy range. The dominance of the  $n = 4$  level is attenuated with increasing impact energies while the  $n = 5$  and  $n \geq 6$  levels see their relative populations increased. At

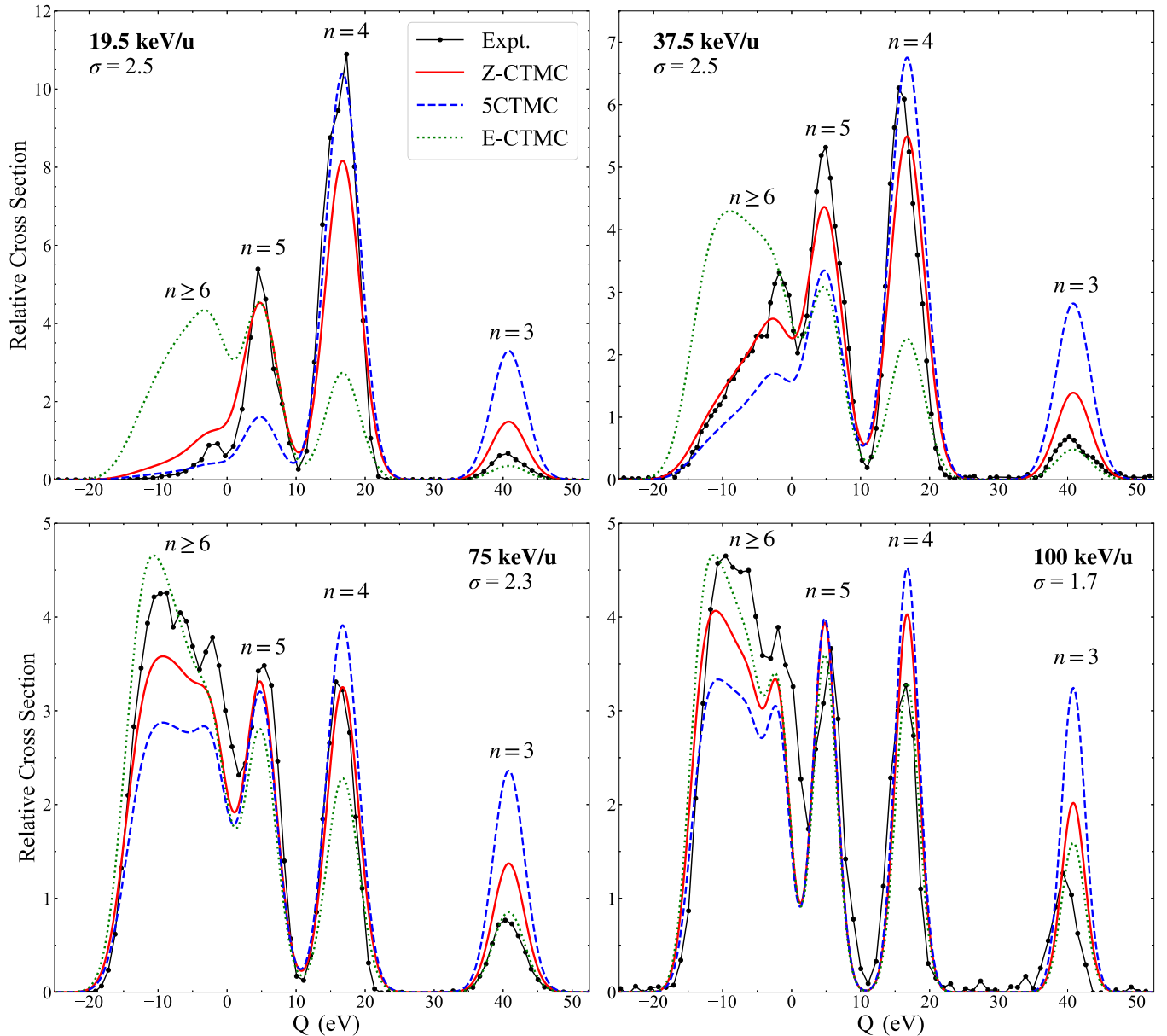


FIG. 3. Nondissociative single electron capture  $Q$  spectra for  $O^{6+}$  collisions on  $H_2$ . The theoretical predictions of the Z-CTMC model are contrasted to those provided by the E-CTMC and 5CTMC methods. The experimental data are those reported in Ref. [37].

100 keV/u the Z-CTMC and E-CTMC distributions are nearly identical.

Since the Z-CTMC is the method that is found in best overall agreement with the data, in Fig. 4(a), we show the total cross section for the sum of the direct one electron capture cross section (nondissociative and dissociative) and the autoionizing double capture (SEC + A2C). In Fig. 4(b) we show the DEC obtained with this method. Present results are compared to the available experimental data and the MCLZ results of Gao *et al.* [48]. For the latter, the authors split their estimated autoionizing double capture contributions assigning 70% of it to SEC and 30% to DEC from their empirical comparison with the data. A fast inspection of these cross sections clearly indicates that the reported MCLZ support the recently reported data by Han *et al.* for the DEC process [35]. However, such data seems to overestimate the data measured

by the JPL data by Machacek *et al.* [32] and the data by Crandall *et al.* [16]. The present Z-CTMC result is in good agreement with the JPL data for DEC at the time they approach the SEC data from below.

### B. State-selective electron capture cross sections in $He^{2+}$ collisions on $H_2$

We now focus on the  $He^{2+}$  projectile, which has been extensively explored either from the experimental and the theoretical sides [19,27,38,72–75]. The idea in this case is to gain insight on whether or not the differences detected among the 5CTMC, E-CTMC, and Z-CTMC models for  $Ne^{9+}$  and  $O^{6+}$  projectiles show up also for a lighter projectile.

In Fig. 5(a) we show the total one-electron capture cross section (SEC+A2C) as a function of impact energy predicted

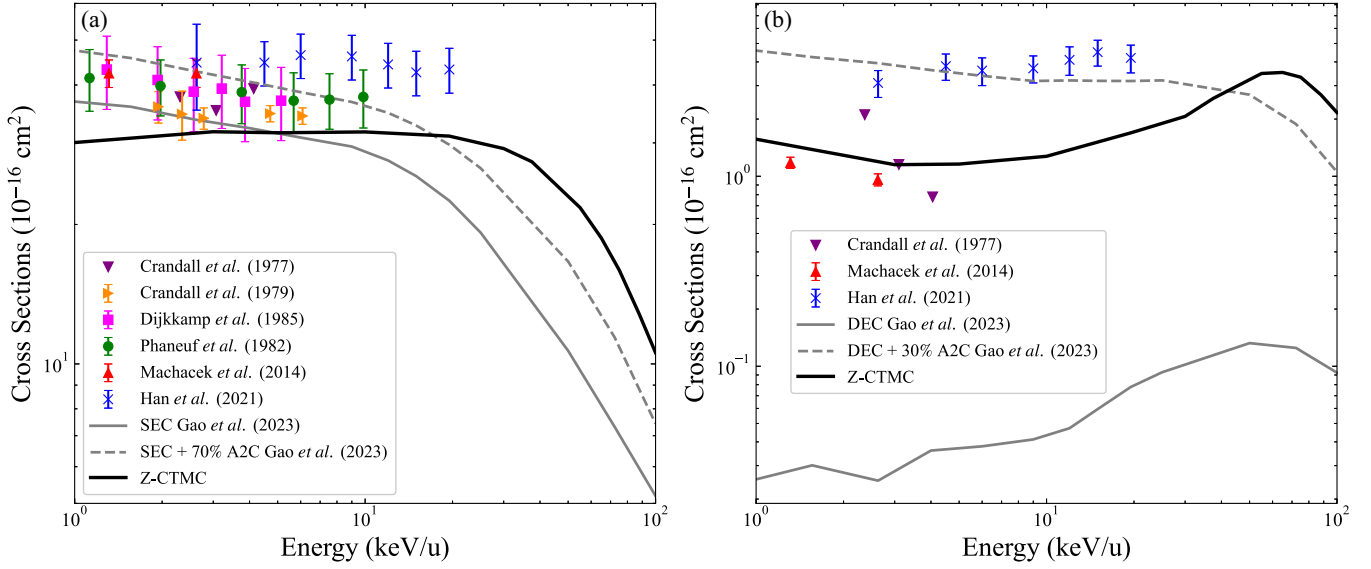


FIG. 4. SEC and DEC total cross sections for  $O^{6+}$  collisions on  $H_2$ . The theoretical predictions of the Z-CTMC model are contrasted to those provided by the MCLZ and the experimental data reported in Ref. [37].

by the 5CTMC, the E-CTMC, and the Z-CTMC methods. The obtained results are compared to the experimental results of Olson *et al.* [38], Shah and Gilbody [19] and Rudd *et al.* [27] at impact energies in the range 7–200 keV/u. It can be seen that the Z-CTMC is in very good agreement, specially with Rudd’s data, at impact energies greater than 10 keV/u. At impact energies lower than 10 keV/u the classical trajectory methods provide a nearly energy-independent behavior and overestimate the experimental data. The E-CTMC method results, in contrast, are in good agreement with the CTMC and Z-CTMC methods at impact energies greater than about 60 keV/u, while it tends to overestimate the experimental data at lower impact energies. We have also added for comparison the semiclassical close-coupling results of Fritsch [72] that

extend up to 100 keV/u and the molecular multicenter CTMC model of Meng *et al.* that covers the 30–200 keV/u impact energy range [39,73]. In Fig. 5(b) we compare our theoretical one-electron capture cross sections to  $He^+(np)$  states with the experimental data and the molecular multicenter CTMC model reported by Meng *et al.* [73]. We observe that the 5CTMC method underestimates the data in all cases, while the E-CTMC method is found in good agreement with the data for the  $2p$  case but tends to overestimate the data for higher  $np$  states at impact energies lower than about 30 keV/u. The Z-CTMC method provides an intermediate behavior between the 5CTMC and the E-CTMC, and is found in overall closer agreement to the theoretical predictions of Meng and the experimental data.

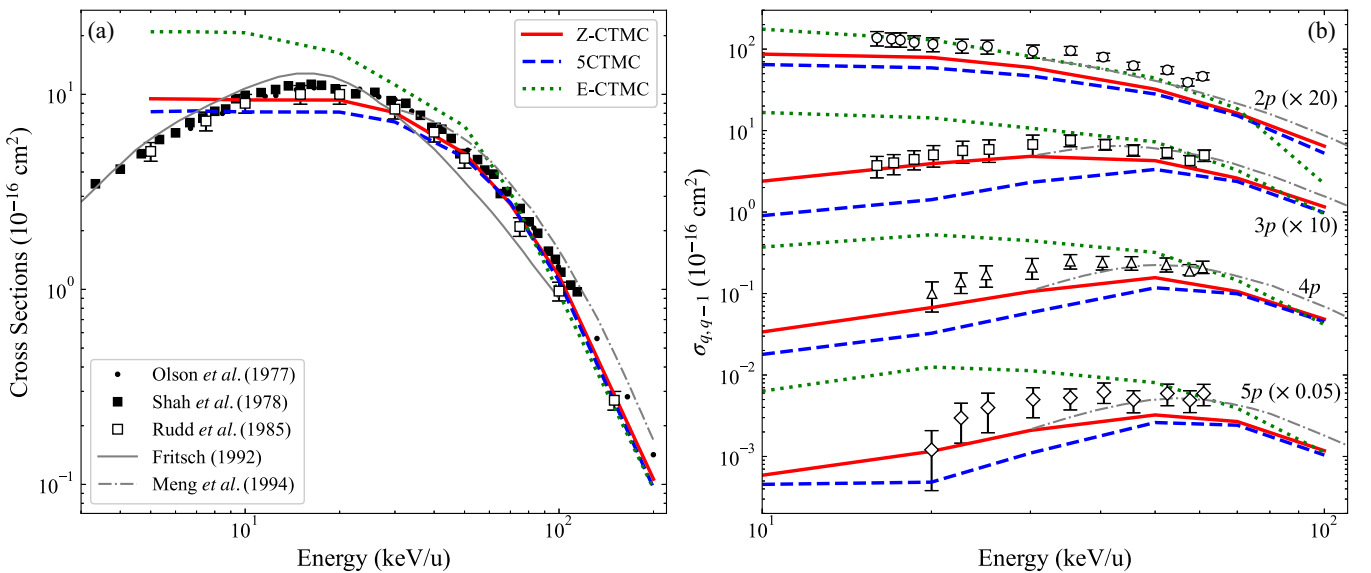


FIG. 5. One-electron capture cross sections following  $He^{2+}$  collisions on  $H_2$  as a function of impact energy: (a) Total cross section (b)  $np$  state selective cross sections. The theoretical predictions of the Z-CTMC model are contrasted to those provided by the 5CTMC method.

TABLE III. Absolute cross sections of the  $n$ -resolved state-selective  $\text{SEC}_{nd}$  process in  $\text{Ne}^{9+}$  collisions with  $\text{H}_2$  in units of  $10^{-16} \text{ cm}^2$ .

Energy (keV/u)	$n$	$\sigma_{\text{Z-CTMC}}$	$\sigma_{\text{5CTMC}}$	$\sigma_{\text{E-CTMC}}$
2.25	4	1.090	1.211	2.490
	5	9.281	8.963	8.902
	6	7.284	1.078	10.49
	7	1.567	0.393	5.499
	$\geq 8$	1.773	0.311	2.389
4.50	4	1.235	1.132	2.762
	5	12.30	14.47	8.966
	6	9.658	0.972	9.819
	7	1.562	0.241	5.211
	$\geq 8$	1.290	0.241	2.293
6.75	4	1.163	1.125	2.827
	5	12.39	15.32	8.782
	6	10.66	0.967	9.425
	7	1.872	0.131	4.573
	$\geq 8$	0.911	0.152	2.156
15.75	4	0.846	0.869	3.001
	5	7.952	7.407	7.754
	6	9.829	2.104	7.913
	7	3.000	0.291	4.649
	$\geq 8$	1.195	0.120	3.238
24.75	4	0.927	0.983	2.806
	5	6.668	5.414	6.758
	6	8.892	2.965	6.797
	7	4.143	0.728	4.101
	$\geq 8$	2.616	0.439	4.527

### C. State-selective electron capture cross sections in $\text{Fe}^{26+}$ collisions on $\text{H}_2$

In this section we consider the  $\text{Fe}^{26+} + \text{H}_2$  collision system at an impact energy of 1 keV/u. Interest in this projectile charge is twofold. On the one hand, differences arising at the

TABLE IV. Comparison of measured and calculated relative cross sections of the  $n$ -resolved state-selective  $\text{SEC}_{nd}$  process in  $\text{O}^{6+}$  collisions with  $\text{H}_2$ .

Energy (keV/u)	$n$	$\sigma_{\text{Expt.}}^{\text{rel}}(\%)$	$\sigma_{\text{Z-CTMC}}^{\text{rel}}(\%)$	$\sigma_{\text{5CTMC}}^{\text{rel}}(\%)$	$\sigma_{\text{E-CTMC}}^{\text{rel}}(\%)$
19.5	3	4.31(0.84)	9.32	20.67	2.22
	4	64.63(2.76)	51.20	65.19	17.15
	5	26.41(1.48)	28.24	10.04	27.92
	$\geq 6$	4.65(1.38)	11.24	4.10	52.71
37.5	3	4.06(0.58)	8.73	17.68	3.03
	4	34.06(2.61)	34.43	42.33	14.13
	5	28.93(2.26)	27.01	20.76	18.89
	$\geq 6$	32.95(8.14)	29.83	19.23	63.95
75	3	4.58(0.32)	7.91	13.61	4.92
	4	17.27(0.73)	18.76	22.56	13.15
	5	18.96(0.79)	18.92	18.31	16.00
	$\geq 6$	59.18(4.86)	54.41	45.52	65.93
100	3	5.48(0.61)	8.60	13.83	6.78
	4	15.63(1.05)	17.18	19.28	14.06
	5	17.05(1.12)	16.79	16.99	15.33
	$\geq 6$	61.84(7.12)	57.43	49.90	63.83

TABLE V. Absolute cross sections of the  $n$ -resolved state-selective  $\text{SEC}_{nd}$  process in  $\text{O}^{6+}$  collisions with  $\text{H}_2$  in units of  $10^{-16} \text{ cm}^2$ .

Energy (keV/u)	$n$	$\sigma_{\text{Z-CTMC}}$	$\sigma_{\text{5CTMC}}$	$\sigma_{\text{E-CTMC}}$
19.5	3	1.387	1.676	0.977
	4	7.621	5.285	7.555
	5	4.203	0.814	12.30
37.5	$\geq 6$	1.666	0.325	23.21
	3	1.182	1.363	0.872
	4	4.664	3.262	4.067
75	5	3.660	1.600	5.436
	$\geq 6$	4.026	1.461	18.39
	3	0.552	0.615	0.397
100	4	1.310	1.019	1.063
	5	1.321	0.827	1.293
	$\geq 6$	3.774	2.013	5.307
100	3	0.328	0.353	0.248
	4	0.656	0.493	0.513
	5	0.641	0.434	0.560
$\geq 6$	2.170	1.232	2.311	

$n$ -state selective SEC cross section from the different physical classical models hereby used are expected to accentuate for such highly charged projectile. On the other hand,  $\text{Fe}^{26+}$  emission lines have been detected at the galactic center and at the galactic ridge [76] thus providing supporting evidence of its relevance for the astrophysical context.

In Fig. 6(a) the  $n$ -state selective SEC cross section is shown. The 5CTMC leads to a narrow structure that peaks at  $n = 11$ . In terms of intensity, the main SEC contributions can be organized in decreasing relevance as follows:  $n = 11, 12, 10, 13$ , and  $14$ . In contrast, the E-CTMC method predicts a wide structure whose maximum is clearly shifted to larger  $n$ -values. In fact, the maximum is attained at  $n = 16$  but similar values are obtained for  $n = 15$  and  $n = 17$ . Such shift is most likely due to the fact that, in its conception, the E-CTMC method recovers the electronic radial distribution by considering an energy distribution for the electron target. Hence, contributions arising from low IP values are expected to enhance the role of larger  $n$  levels as already stated above. On the other hand, the Z-CTMC method predicts a structure with a maximum at  $n_{\text{max}} = 12$ . The distribution is clearly wider than that predicted by 5CTMC, leading to much more intense populations at values larger from  $n_{\text{max}}$ . Theoretical  $n$ -state selective and line emission cross sections obtained by means of the MCLZ method for this collision system have been reported by Mullen *et al.* [50]. These results lead to a maximum at  $n = 12$ . The total SEC cross section for Z-CTMC equals  $8.58 \times 10^{-15} \text{ cm}^2$ , which is lower than that reported MCLZ, but agrees with the extrapolation of the classical trajectory Monte Carlo results by Schultz *et al.* [77].

In order to check whether the previous trends were proper of the  $\text{H}_2$  target, in Fig. 6(b) we perform a similar analysis for atomic hydrogen in the ground state. We observe that the 5CTMC and Z-CTMC methods peak at  $n = 12$ , with the Z-CTMC clearly enhancing the population of  $n > n_{\text{max}}$ . In contrast, the E-CTMC method shows a much wider structure and peaks at  $n = 14$ – $15$ . Therefore, we conclude that the shift

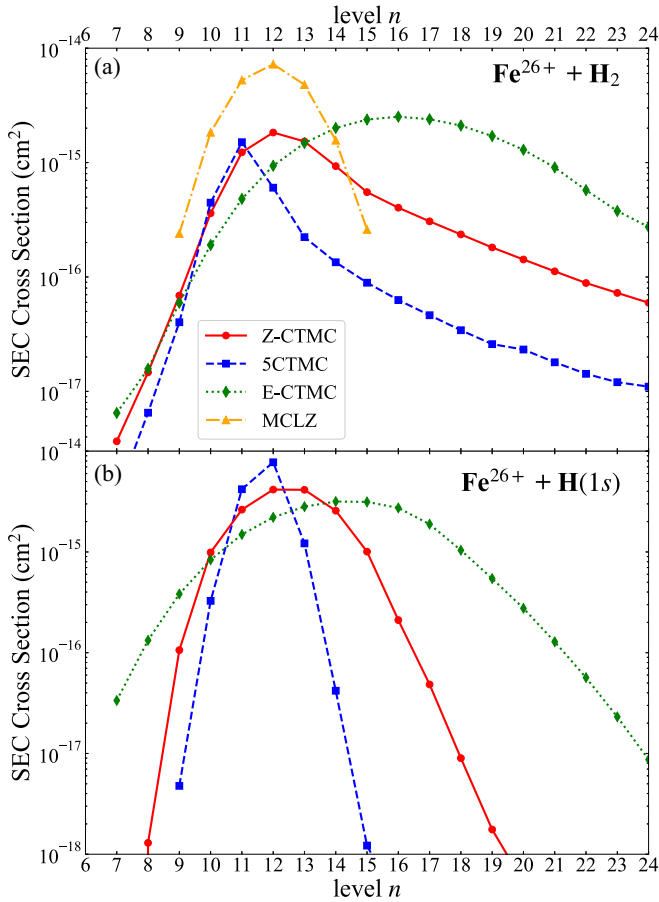


FIG. 6. SEC  $n$ -state selective cross sections for  $\text{Fe}^{26+}$  collisions on  $\text{H}_2$  at an impact energy of 1 keV/u. The theoretical predictions of the Z-CTMC model are contrasted to those provided by the E-CTMC and 5CTMC methods.

of the  $n$  distribution towards larger  $n$  values is not a  $\text{H}_2$  purely related feature, but can be traced to the  $\text{H}(1s)$  description instead. Similarly, the Z-CTMC method leads to the increase of the  $n$  distribution at larger  $n$  values but clearly with less extent.

#### IV. CONCLUSIONS

In this work, two classical trajectory Monte Carlo methods have been introduced to describe collisions between

ions and  $\text{H}_2$  molecules. The spatial distribution of the electrons has been extended to larger distances by incorporating the Z-CTMC and E-CTMC schemes, previously developed for  $\text{H}(1s)$  targets, into the five-body CTMC method developed by Wood and Olson. The procedure hereby introduced reveals the sensitivity of the  $n$ -state selective cross sections to the spatial extension of the electronic distribution, and provides a route to tackle highly charged ions for which precise quantum mechanical data are not available yet or are unfeasible at present due to basis size extension.

The E-CTMC and Z-CTMC models hereby introduced for  $\text{H}_2$ , have been benchmarked against recently reported state-selective experimental data for  $\text{Ne}^{9+}$  and  $\text{O}^{6+}$  projectiles at intermediate to low impact energies. Overall, present results suggest that the Z-CTMC method is the one in closest agreement with the data. Worth noting, and in contrast to the 5CTMC, E-CTMC and the MCLZ methods, the Z-CTMC correctly reproduces the shift of  $n_{\text{max}}$  exhibited by the data in the impact energy range explored. Complementary results for  $\text{He}^{2+}$  projectiles indicate that differences among these models are also visible at lower projectile charges, specially as the impact energy is decreased.

The consideration of a highly charged projectile such as  $\text{Fe}^{26+}$ , indicates that discrepancies among the  $n$ -state selective cross sections predicted by these models accentuate for increasing projectile charges. This situation represents quite a challenge, especially with regard to confidence on the applicability of the cross sections in environments such as the astrophysical.

In summary, present results suggest that the Z-CTMC five-body model provides a valuable tool to analyze collisional processes on  $\text{H}_2$ , such as nondissociative single capture, total one-electron capture, and radiative or autoionizing double capture processes. More experimental data are required at this point, specially regarding highly charged ions, to further test and refine the present theoretical capabilities.

#### ACKNOWLEDGMENTS

Work at IFISUR was supported by Grant No. PGI 24/F084, Secretaría General de Ciencia y Tecnología, Universidad Nacional del Sur.

- [1] C. M. Lisse, K. Dennerl, J. Enghauser, M. Harden, F. E. Marshall, M. J. Mumma, R. Petre, J. P. Pye, M. J. Ricketts, J. Schmitt, J. Trümper, and R. G. West, *Science* **274**, 205 (1996).
- [2] T. E. Cravens, *Geophys. Res. Lett.* **24**, 105 (1997).
- [3] T. E. Cravens, *Astrophys. J.* **532**, L153 (2000).
- [4] P. Beiersdorfer, K. R. Boyce, G. V. Brown, H. Chen, S. M. Kahn, R. L. Kelley, M. May, R. E. Olson, F. S. Porter, C. K. Stahle, and W. A. Tillotson, *Science* **300**, 1558 (2003).
- [5] S. Otranto, R. E. Olson, and P. Beiersdorfer, *Phys. Rev. A* **73**, 022723 (2006).
- [6] S. Katsuda, H. Tsunemi, K. Mori, H. Uchida, H. Kosugi, M. Kimura, H. Nakajima, S. Takakura, R. Petre, J. W. Hewitt, and H. Yamaguchi, *Astrophys. J.* **730**, 24 (2011).
- [7] A. C. Fabian, J. S. Sanders, R. J. R. Williams, A. Lazarian, G. J. Ferland, and R. M. Johnstone, *Mon. Not. R. Astron. Soc.* **417**, 172 (2011).
- [8] K. Dennerl, C. Lisse, A. Bhardwaj, D. Christian, S. Wolk, D. Bodewits, T. Zurbuchen, M. Combi, and S. Lepri, *Astron. Nachr.* **333**, 324 (2012).

- [9] J. Liu, Q. D. Wang, and S. Mao, *Mon. Not. R. Astron. Soc.* **420**, 3389 (2012).
- [10] V. Wakelam, E. Bron, S. Cazaux, F. Dulieu, C. Gry, P. Guillard, E. Habart, L. Hornekaer, S. Morisset, G. Nyman, V. Pirronello, S. D. Price, V. Valdivia, G. Vidal, and N. Watanabe, *Mol. Astrophys.* **9**, 1 (2017).
- [11] C. F. Barnett and P. M. Stier, *Phys. Rev.* **109**, 385 (1958).
- [12] F. De Heer, J. Schutten, and H. Moustafa, *Physica* **32**, 1766 (1966).
- [13] R. Baragiola and I. Nemirovsky, *Nucl. Instrum. Meth.* **110**, 511 (1973).
- [14] M. B. Shah and H. B. Gilbody, *J. Phys. B* **7**, 256 (1974).
- [15] J. E. Bayfield and G. A. Khayrallah, *Phys. Rev. A* **11**, 920 (1975).
- [16] D. H. Crandall, M. L. Mallory, and D. C. Kocher, *Phys. Rev. A* **15**, 61 (1977).
- [17] R. A. Phaneuf, F. W. Meyer, and R. H. McKnight, *Phys. Rev. A* **17**, 534 (1978).
- [18] H. J. Kim, R. A. Phaneuf, F. W. Meyer, and P. H. Stelson, *Phys. Rev. A* **17**, 854 (1978).
- [19] M. B. Shah, T. V. Goffe, and H. B. Gilbody, *J. Phys. B* **11**, L233 (1978).
- [20] F. W. Meyer, R. A. Phaneuf, H. J. Kim, P. Hvelplund, and P. H. Stelson, *Phys. Rev. A* **19**, 515 (1979).
- [21] T. V. Goffe, M. B. Shah, and H. B. Gilbody, *J. Phys. B* **12**, 3763 (1979).
- [22] K. H. Berkner, W. G. Graham, R. V. Pyle, A. S. Schlachter, and J. W. Stearns, *Phys. Rev. A* **23**, 2891 (1981).
- [23] R. A. Phaneuf, I. Alvarez, F. W. Meyer, and D. H. Crandall, *Phys. Rev. A* **26**, 1892 (1982).
- [24] M. E. Rudd, R. D. DuBois, L. H. Toburen, C. A. Ratcliffe, and T. V. Goffe, *Phys. Rev. A* **28**, 3244 (1983).
- [25] M. N. Panov, A. A. Basalae, and K. O. Lozhkin, *Phys. Scr.* **1983**, 124 (1983).
- [26] W. G. Graham, K. H. Berkner, R. V. Pyle, A. S. Schlachter, J. W. Stearns, and J. A. Tanis, *Phys. Rev. A* **30**, 722 (1984).
- [27] M. E. Rudd, T. V. Goffe, and A. Itoh, *Phys. Rev. A* **32**, 2128 (1985).
- [28] D. Dijkkamp, Y. S. Gordeev, A. Brazuk, A. G. Drentje, and F. J. de Heer, *J. Phys. B* **18**, 737 (1985).
- [29] J. B. Greenwood, I. D. Williams, S. J. Smith, and A. Chutjian, *Phys. Rev. A* **63**, 062707 (2001).
- [30] R. J. Mawhorter, J. B. Greenwood, A. Chutjian, T. Haley, C. D. Mitescu, and J. Simcic, *Phys. Rev. A* **84**, 052714 (2011).
- [31] M. Alessi, N. D. Cariatore, P. Focke, and S. Otranto, *Phys. Rev. A* **85**, 042704 (2012).
- [32] J. R. Machacek, D. P. Mahapatra, D. R. Schultz, Y. Ralchenko, A. Chutjian, J. Simcic, and R. J. Mawhorter, *Phys. Rev. A* **90**, 052708 (2014).
- [33] M. Fogle, D. Wulf, K. Morgan, D. McCammon, D. G. Seely, I. N. Draganić, and C. C. Havener, *Phys. Rev. A* **89**, 042705 (2014).
- [34] F. M. Kröger, G. Weber, M. O. Herdrich, J. Glorius, C. Langer, Z. Slavkovská, L. Bott, C. Brandau, B. Brückner, K. Blaum *et al.*, *Phys. Rev. A* **102**, 042825 (2020).
- [35] J. Han, L. Wei, B. Wang, B. Ren, W. Yu, Y. Zhang, Y. Zou, L. Chen, J. Xiao, and B. Wei, *Astrophys. J. Supplement Series* **253**, 6 (2021).
- [36] J. W. Xu, C. X. Xu, R. T. Zhang, X. L. Zhu, W. T. Feng, L. Gu, G. Y. Liang, D. L. Guo, Y. Gao, D. M. Zhao, S. F. Zhang, M. G. Su, and X. Ma, *Astrophys. J. Supplement Ser.* **253**, 13 (2021).
- [37] T. Cao, T. Meng, Y. Gao, S. F. Zhang, R. T. Zhang, S. Yan, X. L. Zhu, J. Wang, P. Ma, B. Ren, Z. H. Xia, D. L. Guo, C. J. Zhang, K. Z. Lin, S. Xu, B. Wei, and X. Ma, *Astrophys. J. Supplement Ser.* **266**, 20 (2023).
- [38] R. E. Olson, A. Salop, R. A. Phaneuf, and F. W. Meyer, *Phys. Rev. A* **16**, 1867 (1977).
- [39] L. Meng, C. O. Reinhold, and R. E. Olson, *Phys. Rev. A* **40**, 3637 (1989).
- [40] G. W. Kerby, M. W. Gealy, Y.-Y. Hsu, M. E. Rudd, D. R. Schultz, and C. O. Reinhold, *Phys. Rev. A* **51**, 2256 (1995).
- [41] C. J. Wood and R. E. Olson, *Phys. Rev. A* **59**, 1317 (1999).
- [42] H. Knudsen, H. K. Haugen, and P. Hvelplund, *Phys. Rev. A* **24**, 2287 (1981).
- [43] M. Gargaud and R. McCarroll, *J. Phys. B* **18**, 463 (1985).
- [44] M. Kimura, S. Chapman, and N. F. Lane, *Phys. Rev. A* **33**, 1619 (1986).
- [45] A. F. Hedrick, T. F. Moran, K. J. McCann, and M. R. Flannery, *J. Chem. Phys.* **66**, 24 (1977).
- [46] R. Shingal and C. D. Lin, *Phys. Rev. A* **40**, 1302 (1989).
- [47] A. Kumar and B. C. Saha, *Phys. Rev. A* **59**, 1273 (1999).
- [48] J. W. Gao, Y. Y. Qi, Y. Wu, and J. G. Wang, *Astrophys. J.* **944**, 167 (2023).
- [49] A. C. K. Leung and T. Kirchner, *Phys. Rev. A* **93**, 052710 (2016).
- [50] P. D. Mullen, R. S. Cumbee, D. Lyons, and P. C. Stancil, *Astrophys. J. Supplement Ser.* **224**, 31 (2016).
- [51] R. S. Cumbee, P. D. Mullen, D. Lyons, R. L. Shelton, M. Fogle, D. R. Schultz, and P. C. Stancil, *Astrophys. J.* **852**, 7 (2018).
- [52] D. Eichenauer, N. Grun, and W. Scheid, *J. Phys. B* **14**, 3929 (1981).
- [53] D. J. W. Hardie and R. E. Olson, *J. Phys. B* **16**, 1983 (1983).
- [54] J. S. Cohen, *J. Phys. B* **18**, 1759 (1985).
- [55] C. Illescas and A. Riera, *Phys. Rev. A* **60**, 4546 (1999).
- [56] N. D. Cariatore, S. Otranto, and R. E. Olson, *Phys. Rev. A* **91**, 042709 (2015).
- [57] N. D. Cariatore, S. Otranto, and R. E. Olson, *Phys. Rev. A* **93**, 066702 (2016).
- [58] K. Igenbergs, J. Schweinzer, A. Veiter, L. Perneczky, E. Frühwirth, M. Wallerberger, R. E. Olson, and F. Aumayr, *J. Phys. B: At., Mol. Opt. Phys.* **45**, 065203 (2012).
- [59] S. Otranto, *Atoms* **11**, 144 (2023).
- [60] S. C. Wang, *Phys. Rev.* **31**, 579 (1928).
- [61] R. L. Becker and A. D. MacKellar, *J. Phys. B* **17**, 3923 (1984).
- [62] A. E. S. Green, D. L. Sellin, and A. S. Zachor, *Phys. Rev.* **184**, 1 (1969).
- [63] R. H. Garvey, C. H. Jackman, and A. E. S. Green, *Phys. Rev. A* **12**, 1144 (1975).
- [64] D. R. Schultz, P. C. Stancil, and M. J. Rakovic, *J. Phys. B: At., Mol. Opt. Phys.* **34**, 2739 (2001).
- [65] R. Ali, C. L. Cocke, M. L. A. Raphaelian, and M. Stockli, *Phys. Rev. A* **49**, 3586 (1994).
- [66] N. D. Cariatore and S. Otranto, *Phys. Rev. A* **88**, 012714 (2013).
- [67] S. Otranto, R. Hoekstra, and R. E. Olson, *Phys. Rev. A* **89**, 022705 (2014).
- [68] H. Tawara, E. Takács, T. Suta, K. Makónyi, L. P. Ratliff, and J. D. Gillaspay, *Phys. Rev. A* **73**, 012704 (2006).

- [69] F. I. Allen, C. Biedermann, R. Radtke, G. Fussmann, and S. Fritzsche, *Phys. Rev. A* **78**, 032705 (2008).
- [70] M. Trassinelli, C. Prigent, E. Lamour, F. Mezdari, J. Mérot, R. Reuschl, J.-P. Rozet, S. Steydli, and D. Vernhet, *J. Phys. B: At., Mol. Opt. Phys.* **45**, 085202 (2012).
- [71] R. E. Olson, *Phys. Rev. A* **24**, 1726 (1981).
- [72] W. Fritsch, *Phys. Rev. A* **46**, 3910 (1992).
- [73] L. Meng, R. E. Olson, H. O. Folkerts, and R. Hoekstra, *J. Phys. B: At., Mol. Opt. Phys.* **27**, 2269 (1994).
- [74] H. F. Busnengo, S. E. Corchs, and R. D. Rivarola, *Phys. Rev. A* **57**, 2701 (1998).
- [75] A. M. Kotian, C. T. Plowman, and A. S. Kadyrov, *Europhys. J. D* **77**, 163 (2023).
- [76] M. P. Muno, F. K. Baganoff, M. W. Bautz, E. D. Feigelson, G. P. Garmire, M. R. Morris, S. Park, G. R. Ricker, and L. K. Townsley, *Astrophys. J.* **613**, 326 (2004).
- [77] D. R. Schultz, L. Meng, C. O. Reinhold, and R. E. Olson, *Phys. Scr.* **1991**, 89 (1991).